buildings

MDPI

Article

Experimental Study of the Seismic Performance of a Prefabricated Frame Rocking Wall Structure

Fuwen Zhang [1], Xiangmin Li [1,*], Zhuolin Wang [1], Kun Tian [1], Kent A. Harries [2] and Qingfeng Xu [1]

[1] Shanghai Key Laboratory of Engineering Structure Safety, Shanghai Research Institute of Building Sciences Co., Ltd., Shanghai 200032, China
[2] Department of Civil and Environmental Engineering, University of Pittsburgh, Pittsburgh, PA 15260, USA
* Correspondence: lixiangmin@sribs.com

Abstract: This paper proposes a prefabricated frame rocking wall (PFRW) structure system in which beams, columns, and rocking walls are all prefabricated components. The rocking wall and the frame are connected by energy-dissipating connectors, and three prestressed tendons are arranged inside the rocking wall. A quasi-static test for the PFRW structure and a conventional frame (CF) structure was conducted. The research results show that the seismic load-resisting capacity of the PFRW structure is increased by about 190% relative to the CF structure, and the energy dissipation coefficient of the PFRW structure is increased to twice that of the CF structure.

Keywords: prefabricated structure; rocking wall; experimental study; quasi-static test; seismic performance

Citation: Zhang, F.; Li, X.; Wang, Z.; Tian, K.; Harries, K.A.; Xu, Q. Experimental Study of the Seismic Performance of a Prefabricated Frame Rocking Wall Structure. *Buildings* **2022**, *12*, 1714. https://doi.org/10.3390/buildings12101714

Academic Editors: Jian Zhong, Xiaowei Wang, Suiwen Wu, Chao Li and Weiping Wen

Received: 6 September 2022
Accepted: 14 October 2022
Published: 17 October 2022

1. Introduction

A rocking wall structure is a structure in which the restraint provided at the base of the wall (connection with foundation) is relaxed or softened. Based on the restraint release and the characteristics of the resulting permitted motion, two types of structure result: In the first, the restraints in the vertical degrees of freedom at the wall base are relaxed, allowing the wall to 'lift' in a vertical direction under the action of an earthquake. The second approach is to relax the rotational degree of freedom at the wall base. While the first approach permits rotation to develop, the second does so without lifting under the action of an earthquake [1]. A rocking wall structure system can change the deformation modes of a structure under earthquake action, mitigating the likelihood of concentrated damage [2]. Rocking wall structures can also affect self-centering functionality, resulting in little or no post-earthquake lateral drift.

Various rocking wall systems have been proposed. Kurama et al. [3] used full wall-height, vertically-oriented unbonded post-tensioned tendons to anchor precast reinforced concrete walls to their foundation. The resulting system allowed the walls to rock under lateral seismic loads, although damage to the system tended to accumulate locally at the wall toes. Ajrab et al. [4] proposed a rocking wall-frame structure in which the shear wall component of the structure was a rocking wall. Ajrab et al. proposed using vertically-draped post-tensioned tendons forming an X-arrangement over the height of the wall. These 'damping cables' were shown to improve the seismic response of the structure. Hitaka et al. [5] proposed a rocking joint shear wall system in which the deformation under the action of an earthquake is mainly concentrated in the wall boundary element consisting of steel coupling beams, reinforced concrete wall limbs, and concrete-filled steel tube side columns.

Because of the nature of the rocking wall mechanism, these systems exhibit relatively low energy absorption [6]. To improve the energy absorption capacity, viscous dampers [7], metal dampers [8,9], and energy-dissipating connectors [10–12] have been proposed for use with rocking wall structures. To mitigate the concentration of damage at the wall

base (primarily the wall toes) associated with rocking [13], Cui et al. [14] proposed an arrangement of steel plates at the bottom of the wall and rubber blocks at the wall toes. Tagliafierro et al. [15] proposed and evaluated the effect of a novel seismic isolation system on seismic control for a steel storage pallet racking system. To improve the self-centering performance of rocking wall structures, a disc spring self-centering device [16] and shape memory alloy self-centering devices [17] have been proposed.

Rocking wall systems have been used in practice. Wada et al. [2] report a rocking wall system used to reinforce an eleven-story building at the Tokyo Institute of Technology, which employed a V-shaped pin support between the base of the rocking wall and the foundation. The support affects an essentially single-pin unrestrained rotational degree of freedom at the wall base. Wu et al. [18] report a rocking wall system used to reinforce a hospital building. In this case, the base of the wall has a connection that limits horizontal lateral movement, while self-centering was realized through post-tensioned tendons.

Extant research on rocking walls primarily focuses on their use in retrofitting existing structures. However, as prefabricated components, rocking walls are particularly well suited for inclusion in prefabricated structures. This results in frame-rocking wall structures having a high prefabrication rate and opens the possibility for the industrialization of such building systems. This paper proposes a prefabricated frame rocking wall (PFRW) system. The beams, columns, and rocking walls are all prefabricated components, while the cast-in-place joint regions of frame components are made robust and ductile through the use of engineered cementitious composites (ECC). Finally, the connection between the rocking wall and frame is made with energy-dissipating connectors. The failure behavior, hysteretic performance, backbone curves, energy dissipation capacity, and residual deformations of the resulting PFRW structure were studied through a pseudo-static reversed-cyclic load test.

2. Experimental Program

Under the lateral load, the frame and the rocking wall in the structure belong to a parallel relationship. Namely, the reaction forces of the frame and the rocking wall in the PFRW are superimposed to resist external loads. The comparison between the single frame without any extra added walls (the CF) and PFRW can better analyze the role played by the rocking wall. Meanwhile, the deformation capacities of the CF and the PFRW are similar due to the constraint between the bottom of the rocking wall, and the base is usually released. Therefore, two concrete structures were fabricated (Figure 1).

The CF structure was entirely cast-in-place (CIP). The PFRW structure consisted of prefabricated components and CIP beam-column connections. Each half-scale frame has three 1500 mm stories and consists of three 1800 mm long bays. Frame CF is the 'control' specimen and the basis of comparison for the second PFRW frame. Precast concrete columns (Figure 1c) are 200 mm square and reinforced with eight 16 mm bars (reinforcing ratio, ρ = 0.04), and confined with 8 mm ties spaced at 100 mm. Precast beams (Figure 1d) are 200 mm $\times$ 120 mm having two 12 mm bars on top and bottom (ρ = 0.017) and 8 mm ties spaced at 100 mm. Column and beam reinforcing bars are made continuous through joint regions using grouted splice sleeves. At the end of beams and tops of columns, straight bar extensions are anchored into extensions of each joint region, as seen in Figure 1a,b. The CIP joint regions are enclosed ECC to enhance the durability and ductility of these regions.

The PFRW specimen replaces the middle frame bay with a 120 mm thickness precast rocking wall (Figure 1b,f). The wall has thirty 8 mm diameter vertical bars (ρ = 0.010) arranged in two layers through the wall thickness, 8 mm horizontal bars at spacings of 50 mm (near the base of the wall), and 100 mm (elsewhere). The reinforcing arrangement also provides eight 8 mm cross ties through the wall thickness coinciding with the horizontal bars. The vertical reinforcement is welded to a continuous steel plate at the base of the wall. Three 15.2 mm diameter unbonded post-tensioning tendons are also provided in the middle region of the wall (Figure 1f); these will provide self-centering capacity for the wall.

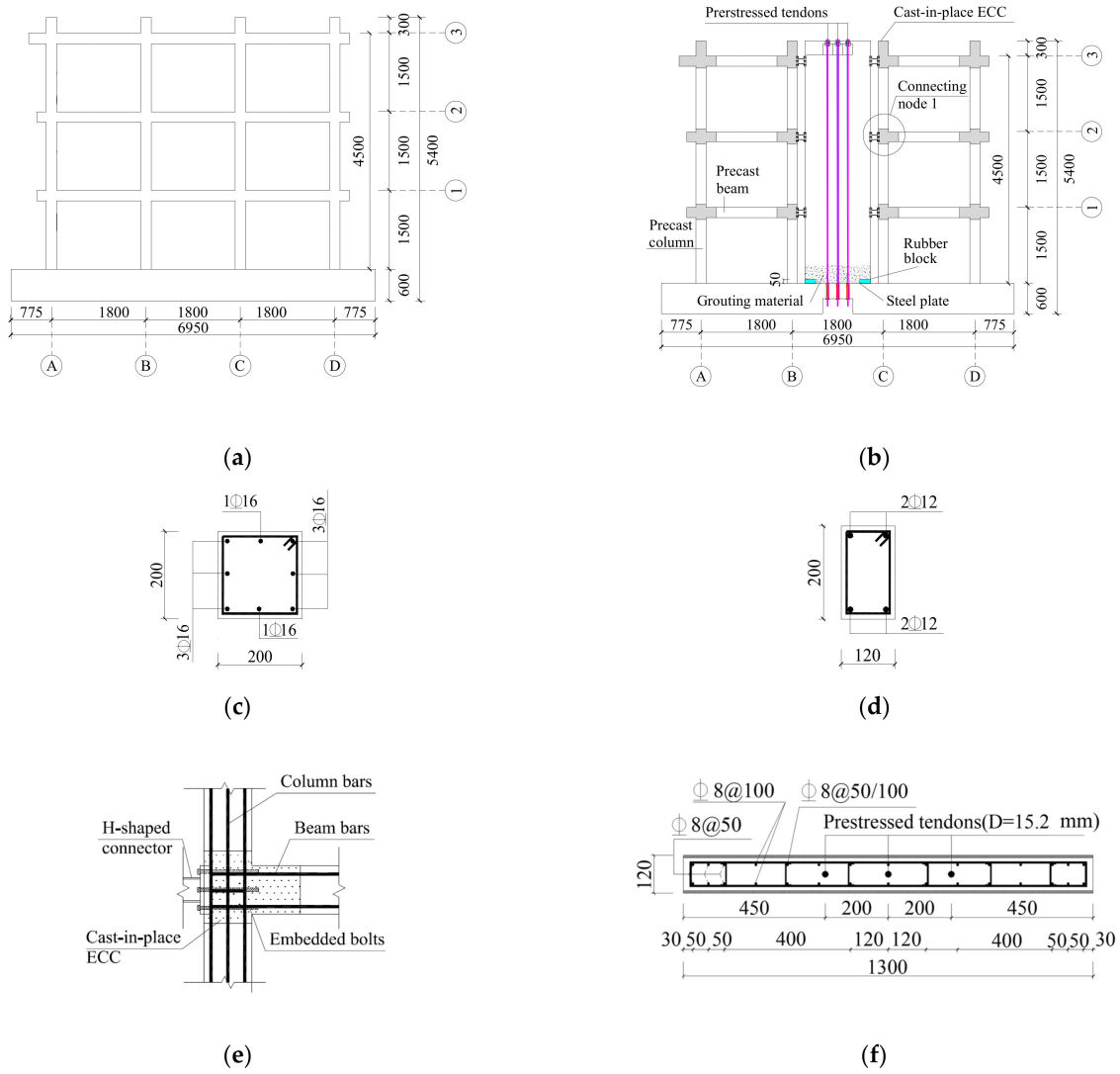

Figure 1. Test specimen dimensions and reinforcement (unit: mm). (**a**) Geometry of CF; (**b**) Geometry of PFRW; (**c**) frame column; (**d**) frame beam; (**e**) typical cast-in-place beam-column connection (connecting node 1); (**f**) rocking wall.

When placed on the foundation, 50 mm tall, 220 mm long neoprene rubber pads are placed at each wall toe. The remaining 860 mm long middle region of the connection is filled with a 50 mm thick course of high-strength cementitious grout. Once assembled, each of the three post-tensioning tendons is stressed to 0.6 f_{ptk}, resulting in a total measured axial prestress force of 442 kN.

The rocking wall is connected to the adjacent frames with the H-shaped energy-dissipating connectors, as shown in Figure 2. The connector is fabricated from a hot-rolled Grade Q235 plate and is designated H100 × 80 × 8 × 8 mm. The H-beam is fully welded to 15 mm end plates and bolted to pre-threaded 25 mm plates embedded in each column-beam joint. The connectors are inserted and secured with six 14 mm diameter bolts at each end plate. Due to the small specimen scale, high-strength cap screws were used in this study rather than high-strength structural (hex) bolts.

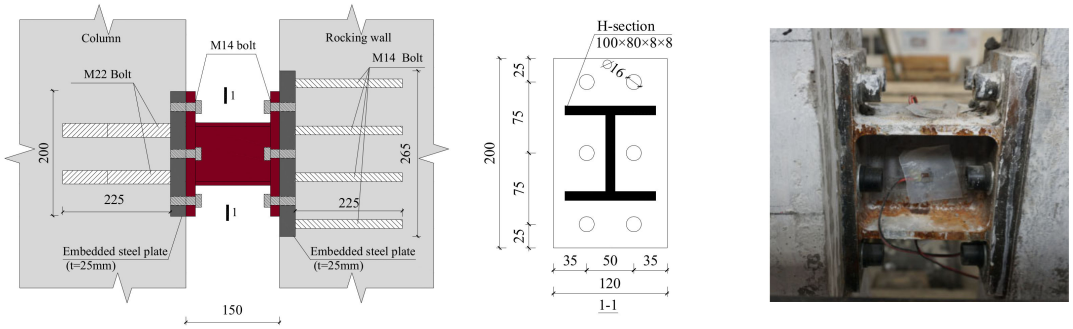

Figure 2. Details of energy-dissipating connector in PFRW (unit: mm). (**a**) Schematic diagram of connecting node; (**b**) Section view of 1–1; (**c**) Photo of connecting node.

2.1. Material Properties

The measured material properties of the concrete, ECC, and high-strength grout used in the specimens are given in Table 1. The ECC had a volume ratio of polyvinyl alcohol (PVA) fiber of 2.5%.

Table 1. Measured cementitious material properties.

	Compression Strength/MPa	Tension Strength/MPa	Tensile Elongation
CF precast columns and beams	38.9	-	-
PFRW columns and beams	40.8	-	-
PFRW rocking wall	43.4	-	-
wall base grout	120.4	-	-
ECC	30.5	3.91	0.025

The rubber blocks had a Shore A hardness of 59, a tensile strength of 20 MPa, a compression modulus of 4.5 MPa, and an elongation at break of 545%. Measured strengths of all reinforcing bars are given in Table 2. The nominal tensile strength of the steel tendon was f_{ptk} = 1860 MPa, and the measured tensile strength and modulus were 1960 MPa and 202 GPa, respectively. The 1000-h relaxation was measured to be 1.54%.

Table 2. Measured strength of reinforcing bar and steel plate.

	Yield Strength/MPa	Ultimate Strength/MPa
6 mm reinforcing bar	408	619
8 mm reinforcing bar	319	520
12 mm reinforcing bar	433	602
16 mm reinforcing bar	411	597
Q235 steel H-section	273	402

2.2. Specimen Loading Protocol

The loading arrangement used is shown in Figure 3. Vertical loads of 143 kN were applied at the top of each column using hydraulic rams. This load is approximately 30% of the column design capacity determined from GB 50010-2010 [19]. This load is applied through a sliding block to remain constant during horizontal load applications. The horizontal load is applied using two servo-hydraulic actuators: one actuator acts at the centerline of the third story beam (i.e., 4400 mm above the foundation block), and the other acts on a distribution beam loading the first and second floor frame beams. The distribution beam is arranged such that it loads the second story beam in a ratio of 2:1 to the first story beam. Both actuators are run at the same load level resulting in a distribution of load to the third:second:first stories = 1:0.66:0.33.

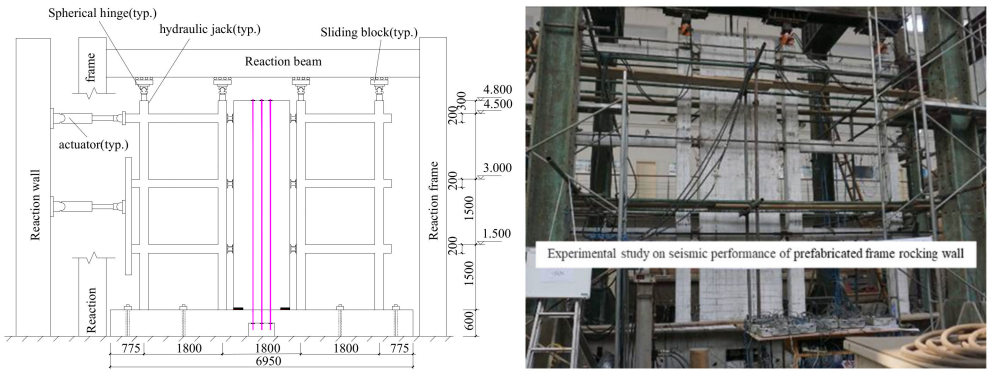

Figure 3. Constant axial load—reversed cyclic lateral load test apparatus. (**a**) Diagram of test loading apparatus; (**b**) Photo of loading apparatus.

Displacement-controlled reversed-cyclic lateral loads are applied to the frames. The third story horizontal displacement is the reference displacement, and the loading sequence is shown in Figure 4. The values in Figure 4 (and elsewhere in this paper) are given in terms of roof drift. The height of the control displacement is H = 4400 mm. In all data, positive represents the actuator "pulling" and negative is "pushing". The first excursion to each displacement level was in the positive direction.

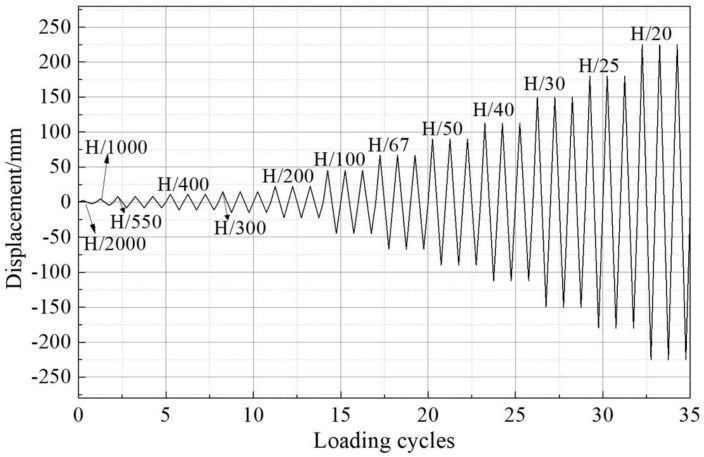

Figure 4. Loading scheme.

The initial cycles to drifts of H/2000 and H/1000 were used to capture the initial cracking state of the frames. Only one loading cycle to these displacements is performed. For the remainder of the test, three fully-reversed cycles for each roof drift were performed.

2.3. Instrumentation

An array of 18 displacement transducers (Figure 5) was used to measure (a) horizontal displacements at each story level, (b) rotation at the base of each column (using vertical transducers at either side of the column), and (c) displacements of the foundation block. For the PFRW specimen, (d) vertical displacement at both rocking wall toes, and (e) horizontal sliding at the base of the rocking wall were also measured. The force in each of the three post-tensioned tendons was also monitored using force sensors in line with the tendon anchorage. Forces in all actuators were also recorded.

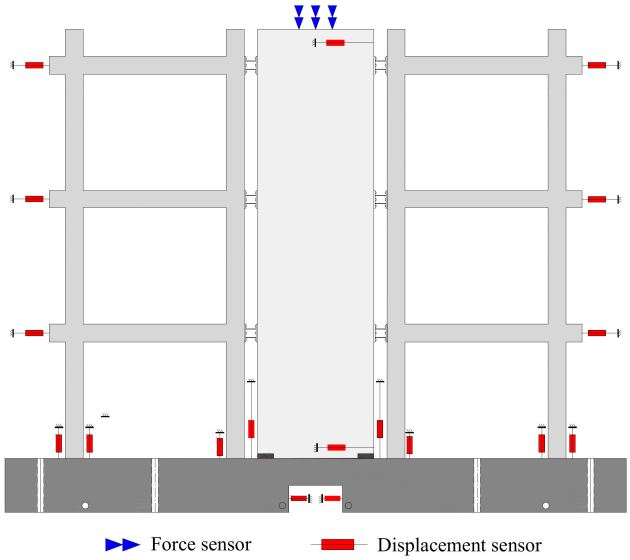

Figure 5. Instrumentation (PFRW shown).

3. Experimental Observations and Comparisons

The total applied horizontal load versus roof drift hysteresis of both frames is shown in Figure 6. The load F is the sum of the actuator forces. Thus, the applied lateral load at the roof level is $F/2$, on the second story: $F/3$, and on the first story: $F/6$.

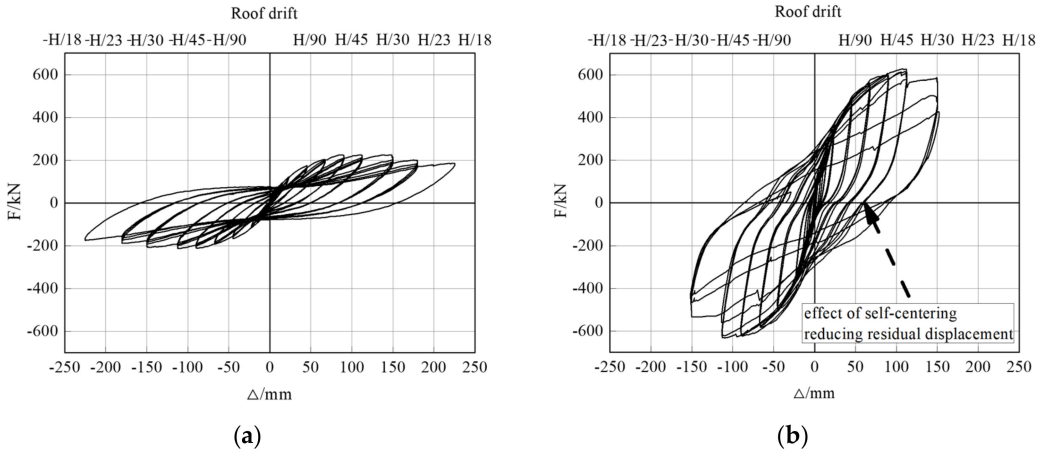

Figure 6. Hysteresis curves of specimens. (**a**) CF structure; (**b**) PFRW structure.

The hysteretic response of the CF structure exhibits a 'pinched' response characterized by limited energy dissipation and large residual displacements as the lateral loading passes through zero. This behavior is well known and reported for reinforced concrete and precast concrete frame systems.

The PFRW structure is, unsurprisingly, stiffer than the CF structure and exhibits little pinching until the final cycles at ±H/30, indicating improved energy dissipation of the structure. The hysteretic response also exhibits a degree of self-centering as the lateral loading passes through zero: from the peak load, the structure initially shows little elastic rebound upon unloading. As the lateral load falls, the self-centering effect of the vertical post-tensioning is seen as a 'horizontal pinching of the hysteresis, as shown in Figure 6b.

3.1. Behavior of CF Structure

The lateral load-roof drift hysteresis of CF is shown in Figure 6a. At a roof drift of ±H/1000, short vertical cracks developed in the tension zone at the beam ends of the

first story. At a drift of ±H/400, horizontal cracks developed at the base of each column. Damage progressed in a relatively uniform manner with continued cycling. The peak lateral load capacity was observed at ±H/40, although this was relatively constant from ±H/50 to ±H/30. At a drift of ±H/25, concrete spalling initiated at the beam ends and column bases (Figure 7a,b), and evidence of buckling of the longitudinal beam bars was seen at the face of the second story exterior column A2 (Figure 7a). At a drift of ±H/20, the lateral load capacity had fallen to 85% of its peak, and the test was ended. A view of frame CF at the –H/20 is shown in Figure 7c, and the final cracking patterns are recorded in Figure 7d. The failure mechanism is dominated by flexural hinges forming in the first and second story beams and at the base of each column.

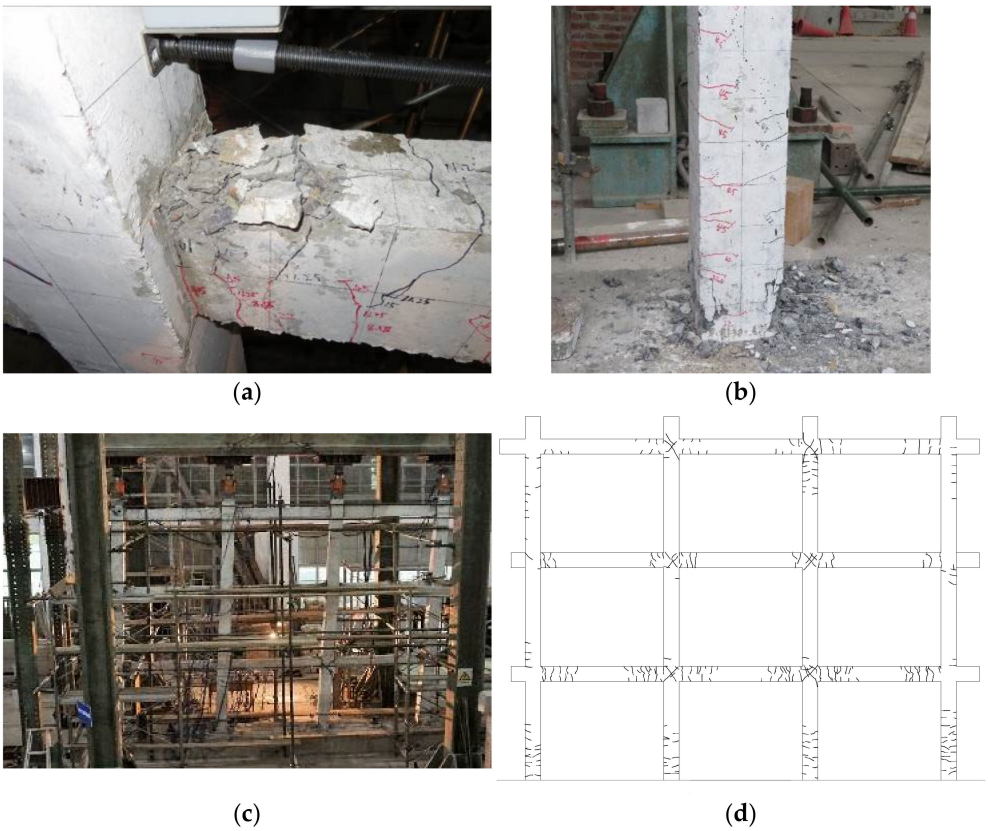

Figure 7. Damage of CF structure. (**a**) damage at second story beam end at face of column A at –H/25; (**b**) damage at base of column A at –H/25; (**c**) overall view of CF at –H/20; (**d**) final crack distribution.

3.2. Behavior of PFRW Structure

The lateral load-roof drift hysteresis of PFRW is shown in Figure 6b. As expected, replacing the middle bay beams with a rocking wall resulted in a considerably stiffer lateral load-resisting system. Initially, at a roof drift of −H/2000, two short vertical cracks developed at the right end (face of column B) of the beam spanning between columns A and B at the first story. At a drift of ±H/550, a crack developed at the base of column B. At a drift of ±H/100, the rocking wall lifting from the foundation at the tension toe, and the energy-dissipating connectors were obviously deformed. Horizontal cracks were evident at the upper and lower edges of the 25 mm embedded steel plates anchoring the connectors. The peak lateral load capacity was observed at ±H/40. By the time a drift of ±H/30 was achieved, all the connectors were significantly damaged (Figure 8a). The concrete at the base of the two middle columns, B and C, was crushed and severely damaged (Figure 8b); the maximum crack width of the column was 3.5 mm. The energy-dissipating connectors were seriously damaged (Figure 8c). The base of the rocking wall exhibited significant uplift, spalling, and cracks up to 0.9 mm wide at the edge of the rubber insert at the wall toe

(Figure 8d). The peak lateral load capacity was observed at ±H/30; the lateral load capacity had fallen to 85% of its peak, and the test ended. A view of frame PFRW at +H/30 is shown in Figure 8d, and the final cracking patterns are recorded in Figure 8f. Due to the similar drift levels, damage to the frame elements was similar to that observed in the CF tests. The energy-dissipating connections of the rocking wall to the frame at each story introduced additional damage at the beam column joints at which the connections were made. Damage to the wall on the second story, primarily to the rocking wall, was also observed but was relatively minor.

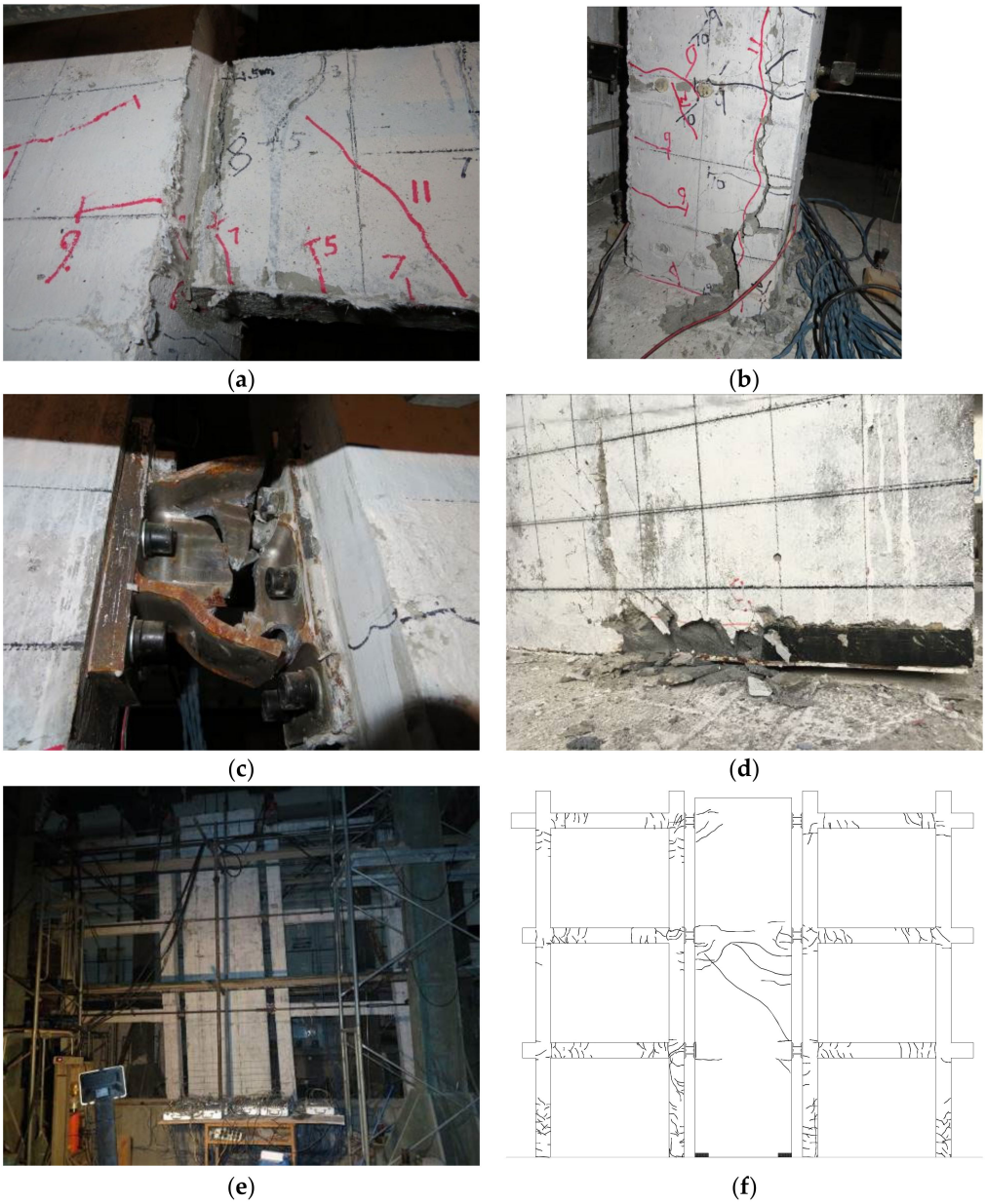

Figure 8. Damage of PFRW structure. (**a**) damage of first story beam at face of column A at +H/30; (**b**) damage at base of column C at +H/30; (**c**) damage to first story energy-dissipating connector at −H/30; (**d**) uplift and spalling at the base of the rocking wall at −H/30; (**e**) overall view of PFRW at −H/30; (**f**) final crack distribution.

3.3. Backbone Curves

A comparison of the backbone curves drawn through the first cycle peaks of frames CF and PFRW is shown in Figure 9. The corresponding key response parameters are

summarized in Table 3. In Table 3, the yield point is determined according to the energy equivalent method [20], $K = F_y/\Delta_y$ is the secant stiffness of the frame defined at the yield point, and $\mu = \Delta_u/\Delta_y$ is the displacement ductility at the ultimate load—defined at 85% of the peak load attained.

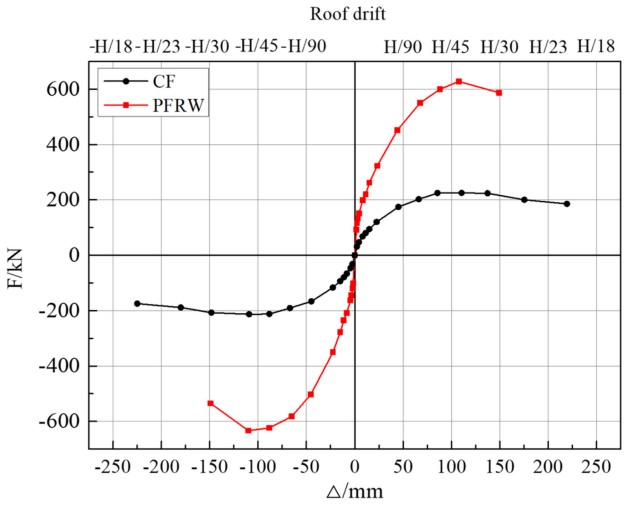

Figure 9. Backbone curves.

Table 3. Key response parameters of the backbone curves.

	Initial Cracking		**Yield**			**Peak Load**		**Ultimate Load at 0.85 F_{max}**		
	F_{cr} /kN	Δ_{cr} /mm	F_y /kN	Δ_y /mm	$K = F_y/\Delta_y$ /kN/mm	F_{max} /kN	Δ_{max} /mm	F_u /kN	Δ_u /mm	$\mu = \Delta_u/\Delta_y$
CF	48.3	4.5 (H/1000)	186.7	54.2 (H/80)	3.4	225.2	110.4 (H/40)	191.4	202.6 (H/20)	3.74
	−47.4	−4.5 (H/1000)	−174.4	−52.2 (H/80)	3.3	−212.7	−109.2 (H/40)	−180.8	−204.8 (H/20)	3.93
PFRW	65.1	3.0 (H/1500)	519.6	60.2 (H/70)	8.6	628.1	107.6 (H/40)	587.3	149.3 (H/30)	2.48
	−80.2	−4.5 (H/1000)	−529.1	−52.0 (H/80)	10.2	−633.1	−110.0 (H/40)	−534.6	−149.1 (H/30)	2.87

Although the stiffness of the PFRW frame increased significantly with the inclusion of the rocking wall—2.8 times based on secant stiffness at yield—the deflections at yield were similar. The rocking wall, therefore, increased the yield load 2.9 times. This observation indicates that the rocking wall was behaving as intended and served to couple the two exterior frames. Had the wall behaved as a shear wall, the stiffness would have been increased, but the yield displacement would likely have fallen due to the limited displacement capacity of conventional shear walls. The significant damage to the energy-dissipating connectors (Figure 8c) reinforces the larger displacements of the rocking wall behavior.

At the peak behavior, observed at the same drift ratio (H/40) in each frame, the capacity of frame PFRW remained about 2.9 times that of frame CF. However, the behavior of the frames near their peak load was different. CF exhibited an extended plateau near its peak load, extending from a drift ratio of approximately H/50 (88 mm) to H/30 (145 mm). In contrast, PFRW exhibited a more defined peak and more 'brittle' behavior, reaching a peak and abruptly losing capacity. The apparent ductility of CF was approximately 1.4 times greater than PFRW.

3.4. Stiffness Degradation

The stiffness degradation of each specimen is calculated as follows:

$$K_i = \sum_{j=1}^{n} F_{j,max}^{i} / \sum_{j=1}^{n} \Delta_j^i \quad (1)$$

where K_i is the stiffness of the cycle, $F_{j,\max}^{i}$ and Δ_j^i are the peak load and corresponding roof displacement, respectively, for the j-th cycle (j = 1 to 3) at the i-th load level. The initial stiffness of each specimen, K_0, is determined for each frame in its pre-cracked state. The evolution of frame stiffness and the degradation curves normalized by K_0 are shown in Figure 10a,b, respectively.

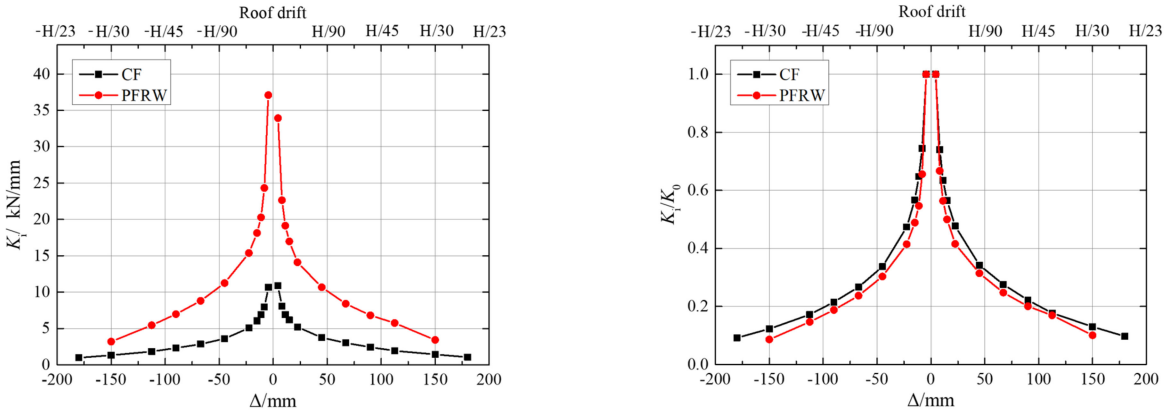

Figure 10. Stiffness degradation of frames. (**a**) evolution of secant stiffness of each frame, K_i; (**b**) stiffness degradation normalized by K_0 for each frame.

Although PFRW is considerably stiffer than CF (Figure 10a), the rate of stiffness degradation is very similar in both specimens. At H/50, lateral stiffness has fallen to about 20% of the initial uncracked stiffness in each frame.

3.5. Energy Dissipation

The energy dissipation of the structure is measured by the area enclosed by the hysteresis curve (i.e., A_{loop}) shown in the inset of Figure 11. The equivalent elastic damping coefficient, β, given by Equation (2), is a measure of the energy absorption characteristics of the hysteresis and is normalized to permit direct comparison [21]. A larger value of β indicates a greater ability to dissipate energy. The maximum theoretical value of β, corresponding to an elastic-perfectly plastic hysteresis, is $2/2\pi = 0.318$.

$$\beta = A_{loop}/2\pi A_e \quad (2)$$

where A_{loop} is the area contained with a single hysteresis loop; and A_e is the area of the triangles defined by the equivalent elastic stiffness to the peak load and displacement of each cycle i; i.e., $A_e{}^i = 0.5\,[F_{i+}\Delta_{i+} + F_{i-}\Delta_{i-}]$.

Figure 11a plots the evolution of energy dissipation with cycling, i.e., the accumulation of A_{loop}. Figure 11b shows the evolution of β with cycling. The upper limit of each band is the first cycle at each drift ratio, and the lower limit is the third. Thus, the width of the data band indicates the deterioration of energy dissipation with cycling.

The absolute energy dissipation of PFRW clearly exceeds that of CF (Figure 11a), as does the rate of increase of energy dissipation of the PFRW structure. The equivalent elastic damping of PFRW also exceeds that of CF (Figure 11b). The equivalent elastic damping coefficient of the PFRW structure levels off at about 110 mm (H/40) lateral deflection, and the difference between the first and third cycles increases substantially. This decay reflects

the rapid deterioration of the energy-dissipating connector (Figure 8c). It is also seen as the dramatic drop in capacity in the hysteresis curve of PFRW at H/30 (Figure 6b).

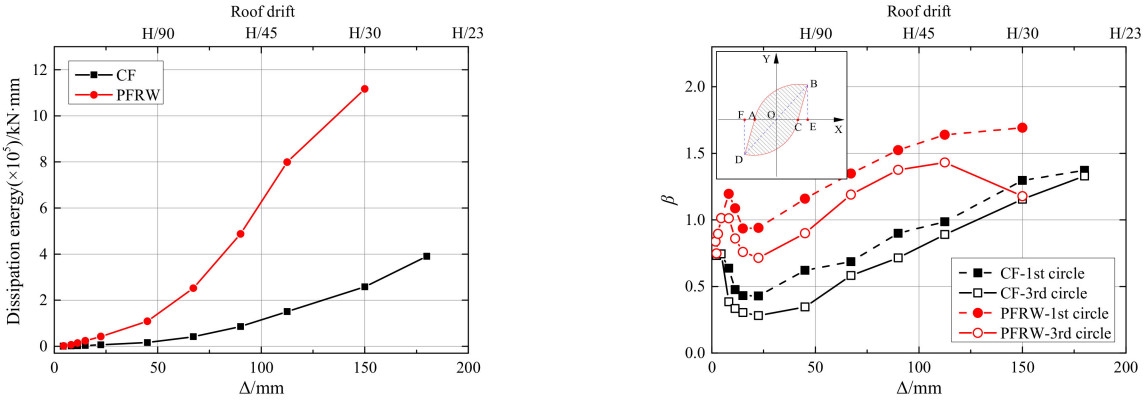

(**a**) (**b**)

Figure 11. Energy dissipation performance of specimens. (**a**) Cumulative energy dissipation; (**b**) equivalent elastic damping.

3.6. Wall Rocking and Residual Displacements

In the PFRW structure, the post-tensioned tendons are the only reinforcement passing across the interface at the base of the wall, connecting the wall with the foundation. Arranged in the middle third of the wall panel, these tendons provide limited resistance to overturning and therefore permit rocking of the wall. Additionally, the post-tensioning force provides a degree of elastic self-centering to the wall. Each tendon was instrumented to monitor the change in load in the tendon throughout the test (Figure 12). The initial force in each tendon was marginally different, as seen in Figure 12: from left to right, the tendons had initial forces of 147 kN, 140 kN, and 154 kN. As seen in Figure 12, these forces increased as the wall toe nearest the tendon experienced tension and eventually uplift (note that the forces for the left and right tendons are out of phase and the middle tendon exhibits less variation). At a roof drift of H/50, the maximum tendon stress has increased by about 25% (right tendon); by failure at H/30, the increase is about 32%. Nonetheless, all tendons remained below 0.8 f_{ptk}. The marginal loss is tendon force during the H/30 cycles reflects the spalling of the wall (Figure 8d) approaching the location of the strand resulting in some relaxation of the strand during the compression cycle.

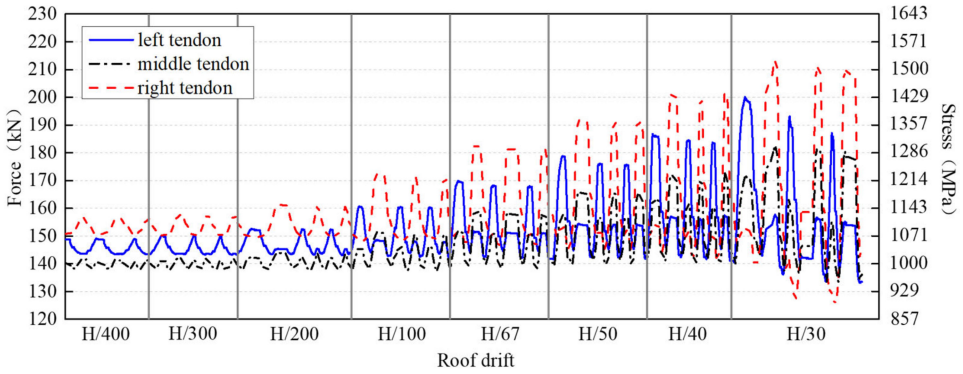

Figure 12. Internal force-time histories of post-tensioning tendons.

The tendons have the effect of self-centering the wall. However, in a wall-frame system, this is 'resisted' by the frame with no self-centering capacity. In the PFRW, the post-tensioned cables are located in the middle third of the wall, giving them a short lever arm and, therefore, a limited ability to generate restoring moments. Only once

the surrounding frames deteriorate significantly, beyond a drift of about H/50, do the effects of self-centering become evident. The restoring moment has not increased; rather, the resistance to self-centering has decreased. Table 4 summarizes the greatest residual deflection observed during selected load cycles. The improved hysteretic behavior of PFRW results in more robust hysteretic loops (Figure 6) and greater relative energy dissipation (Figure 11b). However, the same behavior results in large residual deflections at zero lateral loads. Only as the structure deteriorates, at drifts exceeding H/50, does the benefit of self-centering become apparent, reducing the residual deformation by about 30% at drifts of H/30.

Table 4. Largest residual deformation observed at selected load cycles (unit: mm).

Roof Displacement Drift	H/550	H/300	H/100	H/50	H/40	H/30
CF	1.2	1.4	6.9	33.5	52.0	86.4
PFRW	3.2	5.4	11.2	38.7	45.6	61.2

This last observation has ramifications for PFRW design, indicating a tradeoff between the energy dissipation possible through rocking action and the self-centering capability of the post-tensioned wall pier. That is, efficient self-centering will place the post-tensioned tendons as far from the rocking axis as possible; however, this restrains the rocking behavior.

4. Conclusions

A hybrid precast frame-rocking wall (PFRW) structure is proposed, and a prototypical half-scale model tested under reversed cyclic pseudo-dynamic loading. This structural form was envisioned for new construction but also has the potential for a seismic upgrade retrofit of existing frame structures. To facilitate assembly and reduce the damage to the frame component of the system, engineered cementitious composite (ECC) material was used to form cast-in-place joints between precast beams and columns. The rocking wall component was connected to the frame column using energy-dissipating connectors consisting of short steel beam sections. Three vertical post-tensioning tendons, located in the middle third of the rocking wall, provided a degree of self-centering capacity to the system. The proposed PFRW system was experimentally compared to a frame having the same precast details but no rocking wall component. The following conclusions were drawn:

1. Compared with the CF structure having no rocking wall, the lateral load capacity of the PFRW structure was significantly improved. The greater stiffness of the structure, however, results in marginally reduced drift capacity and reduced displacement ductility;
2. The rocking action engages the energy-dissipating elements connecting the rocking wall to the frame. As a result, the hysteretic response of the PFRW was more robust than that of the frame alone, resulting in not only proportionally greater energy dissipation but (relatively) improved energy dissipation characteristics;
3. In the PFRW, only the rocking wall has self-centering capacity. In this study, only after significant degradation of the frame component was the self-centering evident for the structure itself. The residual displacements of both the PFRW and CF structures were comparable through roof drifts of H/50. Only beyond this—as the frame was damaged—were the residual deformations of the PFRW notably improved;
4. The combination of conclusions 2 and 3 highlights the compromise the designer must make between the energy dissipation possible through rocking action and the self-centering capability of the post-tensioned wall pier. That is, efficient self-centering will place the post-tensioned tendons as far from the rocking axis as possible; however, this restrains the rocking behavior.

Author Contributions: Formal analysis, Z.W.; investigation, F.Z.; resources, X.L.; data curation, K.T.; writing—original draft preparation, K.T.; writing—review and editing, K.A.H. and Q.X.; supervision, X.L., K.A.H. and Q.X.; project administration, F.Z. All authors have read and agreed to the published version of the manuscript.

Funding: This work was financially sponsored by Program of Shanghai Technology Research Leader (21XD1432800), State Key Laboratory of Disaster Reduction in Civil Engineering (SLDRCE20-03), and Natural Science Foundation of Shanghai (20ZR1424500).

Data Availability Statement: Not applicable.

Acknowledgments: The authors are greatly indebted to the anonymous reviewers for their valuable comments and suggestions, which helped in improving the overall quality of this manuscript greatly.

Conflicts of Interest: The authors declare no conflict of interest.

References

1. Zhou, Y.; Wu, H.; Gu, A.Q. Earthquake engineering: From earthquake resistance, energy dissipation, and isolation, to resilience. *Eng. Mech.* **2019**, *36*, 1–12. (In Chinese)
2. Wada, A.; Qu, Z.; Ito, H.; Motoyui, S.; Sakata, H.; Kasai, K. Seismic retrofit using rocking walls and steel damper. In *Improving the Seismic Performance of Existing Buildings and Other Structures*; American Society of Civil Engineers: San Francisco, CA, USA, 2009; pp. 1010–1021.
3. Kurama, Y.; Sause, R.; Pessiki, S.; Lu, L.W. Lateral load behavior and seismic design of unbonded post-tensioned precast concrete walls. *ACI Struct. J.* **1999**, *96*, 622–633.
4. Aiorab, J.; Pekcan, G.; Mander, J. Rocking wall-frame structures with supplemental tendon systems. *J. Struct. Eng.* **2004**, *130*, 895–903.
5. Hitaka, T.; Sakino, K. Cyclic tests on a hybrid coupled wall utilizing a rocking mechanism. *Earthq. Eng. Struct. Dyn.* **2008**, *37*, 1657–1676. [CrossRef]
6. Yoorasertchai, E.; Warnitchai, P. Seismic performance of precast hybrid moment-resisting frame/rocking wall systems. *Mag. Concr. Res.* **2018**, *70*, 1118–1134.
7. Wight, G.; Ingham, J.; Kowalsky, M. Shake table testing of rectangular post-tensioned concrete masonry walls. *ACI Struct. J.* **2006**, *103*, 587–595.
8. Toranzo, L.A.; Restrepo, J.I.; Mander, J.B.; Carr, A.J. Shake-Table Tests of Confined-Masonry Rocking Walls with Supplementary Hysteretic Damping. *J. Earthq. Eng.* **2009**, *13*, 882–898. [CrossRef]
9. Marriott, D.; Pampanin, S.; Palermo, A. Quasi-static and pseudo-dynamic testing of unbonded post-tensioned rocking bridge piers with external replaceable dissipaters. *Earthq. Eng. Struct. Dyn.* **2009**, *38*, 331–354. [CrossRef]
10. Nazari, M.; Sritharan, S. Seismic design of precast concrete rocking wall systems with varying hysteretic damping. *PCI J.* **2019**, *64*, 58–76. [CrossRef]
11. Sritharan, S.; Aaleti, S.; Henry, R.S.; Liu, K.-Y.; Tsai, K.-C. Precast Concrete Wall with End Columns (PreWEC) for Earthquake Resistant Design. *Earthq. Eng. Struct. Dyn.* **2015**, *44*, 2075–2092. [CrossRef]
12. Restrepo, I.; Rahman, A. Seismic performance of self-centering structural walls incorporating energy dissipaters. *J. Struct. Eng.* **2007**, *133*, 1560–1570. [CrossRef]
13. Lu, X.L.; Wu, H. Study on seismic performance of prestressed precast concrete walls through cyclic lateral loading test. *Mag. Concr. Res.* **2017**, *69*, 1–14. [CrossRef]
14. Cui, H.; Wu, G.; Zhang, J.; Xu, J. Experimental study on damage-controllable rocking walls with resilient corners. *Mag. Concr. Res.* **2019**, *71*, 1113–1129. [CrossRef]
15. Tagliafierro, B.; Montuori, R.; Castellano, M.G. Shake table testing and numerical modelling of a steel pallet racking structure with a seismic isolation system. *Thin-Walled Struct.* **2021**, *164*, 107924. [CrossRef]
16. Jiang, L.; Li, X.M.; Zhang, F.W.; Dong, J.Z.; Jiang, L.X.; Xu, Q.F. Experimental investigation on seismic performance of frame-rocking wall structures using disc springs. *J. Build. Struct.* **2019**, *40*, 61–70. (In Chinese)
17. Dong, J.Z.; Li, X.M.; Zhang, F.W.; Jiang, L.X.; Jiang, L.; Xu, Q.F. Experimental study on seismic performance of frame-controlled rocking wall structures using SMA devices. *China Civil Eng. J.* **2019**, *52*, 41–51. (In Chinese)
18. Wu, S.J.; Pan, P.; Zhang, X. Characteristics of frame rocking wall structure and its application in a seismic retrofit. *Eng. Mech.* **2016**, *33*, 54–60+67. (In Chinese) [CrossRef]
19. *GB50010-2010(2015)*; Code for Design of Concrete Structures. China Architecture and Building Press: Beijing, China, 2015.
20. Ma, F.; Deng, M.; Ma, Y.; Lü, H.; Yang, Y.; Sun, H. Experimental study on interior precast concrete beam–column connections with lap-spliced steel bars in field-cast RPC. *Eng. Struct.* **2021**, *228*, 111481. [CrossRef]
21. Clough, R.W.; Penzien, J. *Dynamics of Structures*; McGraw-Hill Education: New York, NY, USA, 1993.